Three-spin coherent oscillations and interference

Poulin-Lamarre, G.; Thorgrimson, J.; Studenikin, S. A.; Aers, G. C.; Kam, A.; Zawadzki, P.; Wasilewski, Z. R.; Sachrajda, A. S.

Publisher's version / Version de l'éditeur:
https://doi.org/10.1103/PhysRevB.91.125417
Physical Review B - Condensed Matter and Materials Physics, 91, 12, 2015-03-16

Three-spin coherent oscillations and interference

G. Poulin-Lamarre,[1,2] J. Thorgrimson,[1,3] S. A. Studenikin,[1] G. C. Aers,[1] A. Kam,[1] P. Zawadzki,[1]
Z. R. Wasilewski,[1] and A. S. Sachrajda[1,*]

[1]*National Research Council Canada, Ottawa, Ontario K1A 0R6, Canada*
[2]*Département de physique, Université de Sherbrooke, Sherbrooke, Québec J1K 2R1, Canada*
[3]*Department of Physics, McGill University, 3600 rue University, Montréal, Québec H3A 2T8, Canada*

(Received 20 November 2013; revised manuscript received 18 February 2015; published 12 March 2015; corrected 16 March 2015)

We utilize magnetic field dependencies to identify two hitherto unobserved quantum interference processes in a triple quantum dot circuit. The first observation involves the interplay of Landau-Zener-Stückelberg behavior from two separate anticrossings between two energy levels that anticross twice as a function of a detuning parameter. The second process involves quantum interference between all-exchange and hyperfine qubits activated in a three-spin system.

DOI: 10.1103/PhysRevB.91.125417 PACS number(s): 73.63.Kv, 03.67.−a, 73.21.La

I. INTRODUCTION

Recently, the triple quantum dot (TQD) system has been intensely analyzed theoretically [1–5] motivated by the potential advantages of three-spin states as qubits and the fact that even the simplest algorithms and certain functionalities, such as spin buses, require a TQD for a proof of concept demonstration. Experimentally, the fundamental properties of linear TQD devices have been successfully measured [6–12]. This has culminated in the recent observation of both Landau-Zener-Stückelberg (LZS) interferometry [10] (originally demonstrated with double dots [13]) and the all-exchange (AE) qubit [11,12]. In particular, the AE spin qubit has the distinct advantage that all required Bloch sphere rotations can be achieved entirely via electrical control of the exchange interaction.

The TQD energy level spectrum is more complex than its double dot counterpart, providing several potential coherent leakage paths away from any desired qubit basis. Motivated by this we have studied the coherent response of a three-spin system to different pulse characteristics. This involves a detailed analysis of magnetic field dependencies, a technique previously used by us to observe the AE qubit [11]. In this paper we identify two previously unobserved quantum interference phenomena in the system. The first was predicted but not observed [11] and is based on an interplay between two interrelated spin LZS interferometers. The second involves an interference process between the AE and LZS qubits. We term these double beam splitter (DBS) and exchange-enabled LZS (e-LZS) interferences, respectively. In addition to being interesting phenomena in their own right these intricate coherent evolutions need to be understood for their consequences on qubit purity.

In Sec. II we discuss the states of a triple dot related to our experiments, our density matrix calculations for comparison with experimental measurements, and the calibration method to extract the required exchange energies to model the system. In Sec. III we review the observation of AE and LZS coherent oscillations as a function of applied magnetic field. Section IV describes the appearance of double beam splitter and exchange-enabled LZS interferences together with illustrations of the corresponding state evolutions.

II. TRIPLE DOT STATES

Here we first review the relevant states of a triple quantum dot and our experimental and theoretical approaches to observing interference effects between them. Our linear TQD device has been discussed elsewhere [10]. It is shown in the bottom inset to Fig. 1(a). Gate C tunes the (1,1,1) region size. Gates 1 and 2 were used to control the charge state of the device and to manipulate the tunneling between the dots. They were connected to high-frequency circuitry used for the applications of pulses. Nearby quantum point contacts (QPCs) were used to measure the TQD charge configuration using standard techniques [14].

Figure 1(a) displays a typical charge detection stability diagram obtained under DC conditions around the relevant (2,0,1), (1,1,1) and (1,0,2) regime [(N_L,N_C,N_R) denote the occupation of left, center, and right quantum dots, respectively].

In Fig. 1(c), we plot a schematic energy level diagram along a detuning (ϵ) line from (2,0,1) to (1,0,2) [zero detuning is defined to be at the center of the (1,1,1) region]. We follow the terminology of Laird *et al.* [9] to describe the three-electron-spin system which can be characterized by eight states, divided into two spin subgroups, offset by the Zeeman energy E_z: four quadruplet states Q_{S_z} with total spin $S = 3/2$ ($S_z = \pm 3/2, \pm 1/2$) and two pairs of doublet states Δ_{S_z} and Δ'_{S_z} with total spin $S = 1/2$ ($S_z = \pm 1/2$). Here, we consider only the positive S_z subset of states [13,15,16]. These can be written as:

$$|Q_{1/2}\rangle = \frac{1}{\sqrt{3}}(|\uparrow\uparrow\downarrow\rangle + |\uparrow\downarrow\uparrow\rangle + |\downarrow\uparrow\uparrow\rangle) \tag{1}$$

$$|\Delta_{1/2}\rangle = F_\Delta((J_{LC} - J_{RC} + \Omega)|\uparrow\uparrow\downarrow\rangle + (J_{RC} - \Omega)|\uparrow\downarrow\uparrow\rangle - J_{LC}|\downarrow\uparrow\uparrow\rangle) \tag{2}$$

$$|Q_{3/2}\rangle = |\uparrow\uparrow\uparrow\rangle \tag{3}$$

$$|\Delta'_{1/2}\rangle = F_{\Delta'}((-J_{LC} + J_{RC} + \Omega)|\uparrow\uparrow\downarrow\rangle - (J_{RC} + \Omega)|\uparrow\downarrow\uparrow\rangle + J_{LC}|\downarrow\uparrow\uparrow\rangle), \tag{4}$$

where $\Omega = \sqrt{J_{LC}^2 + J_{RC}^2 - J_{LC}J_{RC}}$, $F_\Delta = 1/\sqrt{4\Omega^2 + 2\Omega(J_{LC} - 2J_{RC})}$, and

*Andrew.Sachrajda@nrc.ca

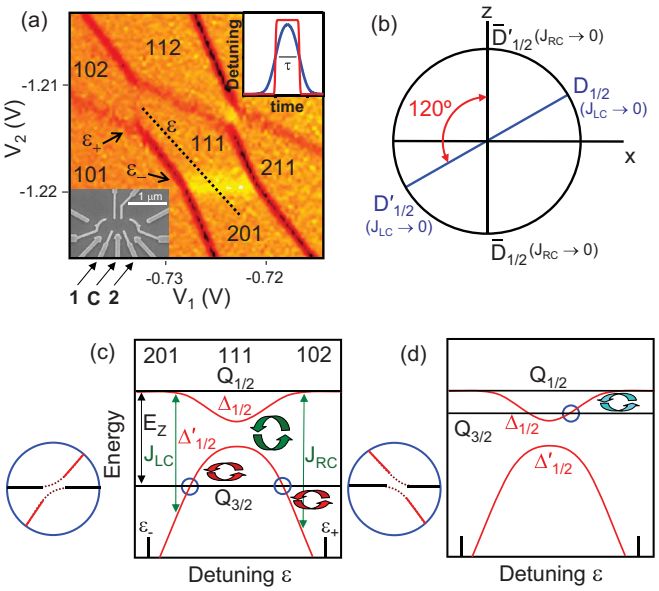

FIG. 1. (Color online) (a) Charge stability diagram in the relevant spin qubit regime [7]. A typical detuning span (dotted line) for pulses used in the experiments is indicated. Bottom inset shows an electron micrograph of the device. Top inset shows gate pulse shapes for two rise times at fixed duration τ. (b) Bloch sphere x-z cross section in the $\bar{D}'_{1/2}$-$\bar{D}_{1/2}$ basis (the all-exchange qubit). (c) Schematic of three-spin energies for the relevant states as a function of detuning. ϵ_- and ϵ_+ denote positions of charge transfer lines. Small circulation symbols (red) denote coherent LZS oscillations produced by pulse from (2,0,1) region across anticrossings denoted by blue circles (anticrossings expanded in accompanying graphics) where $Q_{3/2}$ cuts $\Delta'_{1/2}$. Large green circulation symbol indicates $\Delta'_{1/2}/\Delta_{1/2}$ exchange oscillations. (d) Same as (c) but for lower magnetic field such that $Q_{3/2}$ cuts $\Delta_{1/2}$. Circulation symbol: e-LZS generated from right side anticrossing.

$F_{\Delta'} = 1/\sqrt{4\Omega^2 + 2\Omega(2J_{RC} - J_{LC})}$. $J_{LC}[J_{RC}]$ are the exchange energies for the left-center (right-center) dot pairs. The corresponding energies of these states are:

$$E_{Q_{1/2}} = -E_z/2 \tag{5}$$

$$E_{\Delta_{1/2}} = -(J_{LC} + J_{RC} - \Omega + E_z)/2 \tag{6}$$

$$E_{Q_{3/2}} = -3E_z/2 \tag{7}$$

$$E_{\Delta'_{1/2}} = -(J_{LC} + J_{RC} + \Omega + E_z)/2 \tag{8}$$

with $E_z = g^*\mu_B B$ where μ_B is the Bohr magneton and $g^* = -0.44$ is the GaAs electron g factor.

In the limits of large $|\epsilon|$, where the pulses start and end and where one or other of the two exchange terms J_{LC} or J_{RC} approximates 0, the $\Delta'_{1/2}$ ($\Delta_{1/2}$) doublet state evolves to the $-\bar{D}'_{1/2}$ ($-\bar{D}_{1/2}$) and $D'_{1/2}$ ($D_{1/2}$) states of Ref. [9] respectively on the left and right side of Figs. 1(c), 1(d). For example, on the left side of Figs. 1(c), 1(d), where the detuning favors the transfer of the center electron to the left dot, the $\bar{D}'_{1/2}$ state consists essentially of a singlet on the left-center dots with a spectator up-spin on the right dot. Likewise, the $\bar{D}_{1/2}$ and $Q_{1/2}$ states can be viewed as a linear combinations of T_o and T_+ triplets on the left-center dots with different spins on the right dot:

$$|\bar{D}_{1/2}\rangle = \frac{-1}{\sqrt{6}}(2|\uparrow\uparrow\downarrow\rangle - |\uparrow\downarrow\uparrow\rangle - |\downarrow\uparrow\uparrow\rangle)$$

$$= \frac{-1}{\sqrt{3}}(\sqrt{2}|T_+\rangle_{LC}|\downarrow\rangle - |T_o\rangle_{LC}|\uparrow\rangle) \tag{9}$$

$$|\bar{D}'_{1/2}\rangle = \frac{1}{\sqrt{2}}(|\uparrow\downarrow\uparrow\rangle - |\downarrow\uparrow\uparrow\rangle) = |S\rangle_{LC}|\uparrow\rangle. \tag{10}$$

Similarly, on the right side of Figs. 1(c), 1(d), where the detuning favours the transfer of the center electron to the right dot, the $D'_{1/2}$ state consists essentially of a singlet on the right-center dots with a spectator up-spin on the left dot and the $D_{1/2}$ and $Q_{1/2}$ states can be viewed as a linear combinations of T_o and T_+ triplets on the right-center dots with different spins on the left dot:

$$|D_{1/2}\rangle = \frac{-1}{\sqrt{6}}(2|\downarrow\uparrow\uparrow\rangle - |\uparrow\downarrow\uparrow\rangle - |\uparrow\uparrow\downarrow\rangle)$$

$$= \frac{-1}{\sqrt{3}}(\sqrt{2}|\downarrow\rangle|T_+\rangle_{RC} - |\uparrow\rangle|T_o\rangle_{RC}) \tag{11}$$

$$|D'_{1/2}\rangle = \frac{1}{\sqrt{2}}(|\uparrow\uparrow\downarrow\rangle - |\uparrow\downarrow\uparrow\rangle) = |\uparrow\rangle|S\rangle_{RC}. \tag{12}$$

For this reason (in these limits) the standard double dot spin to charge detection readout technique based on the Pauli exclusion principle and singlet and triplet states can also be used in TQDs [15,17].

The two sets of D states $\bar{D}'_{1/2}$, $\bar{D}_{1/2}$, and $D'_{1/2}$, $D_{1/2}$ are simply related and can thus be represented on the same Bloch sphere in the $\bar{D}'_{1/2}$, $\bar{D}_{1/2}$ basis as shown in Fig. 1(b) but with axes rotated by 120° (this angle originating from the coefficients of $D'_{1/2}$, $D_{1/2}$ expressed in the $\bar{D}'_{1/2}$, $\bar{D}_{1/2}$ basis). Thus for the all-exchange qubit, $\Delta'_{1/2}$-$\Delta_{1/2}$ [see Fig. 1(c)], all positions on the Bloch sphere can be reached with a combination of J_{LC} and J_{RC} rotations around these two axes, generated by detuning pulses to each side of Figs. 1(c), 1(d).

The x, y components of the fluctuating nuclear hyperfine field gradients between the dots split the two $\Delta'_{1/2}/Q_{3/2}$ crossings shown in Fig. 1(c), creating the anticrossings responsible for the LZS behavior described in this paper while the z components lead to additional coupling of the $Q_{1/2}$ state to $\Delta_{1/2}$ and $\Delta'_{1/2}$ [12,16].

The dotted line on the stability diagram [Fig. 1(a)] marks a typical trajectory of the voltage pulses used in this paper starting and finishing in (2,0,1). For the experiments described here we employ a rectangular voltage pulse of duration τ and amplitude $(\delta V_1, \delta V_2)$ filtered with a finite rise time [Fig. 1(a) top inset]. We define the initial detuning (the detuning position at the start and the end of the pulse) as dV_2 along V_2 relative to zero detuning. This is the parameter plotted as the Y axis in Figs. 2–4, 7. Spin to charge conversion is used for spin projection measurements in the (2,0,1) region to obtain the doublet occupation probability $P_{\bar{D}'_{1/2}}$ [17].

Throughout this paper we model the spin state evolution in response to the voltage pulses from calculations of the time dependence $d\rho/dt = i[\rho, H/\hbar]$ of the density matrix ρ in the $Q_{1/2}/\bar{D}_{1/2}/Q_{3/2}/\bar{D}'_{1/2}$ basis starting from an initial state at large negative detuning where $P_{\bar{D}'_{1/2}} = 1$ [10]. The resulting

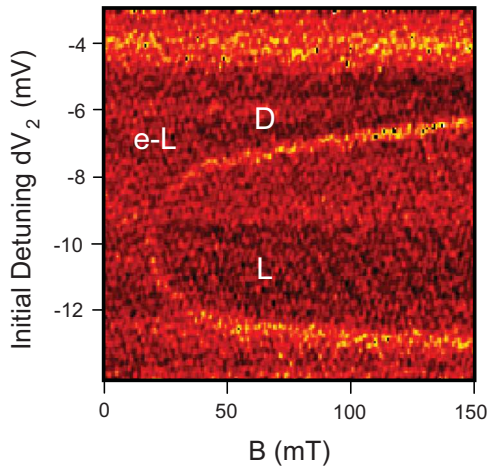

FIG. 2. (Color online) Typical measurement used to extract the interdot exchange couplings, required for simulations, from the locus of $Q_{3/2}/\Delta'_{1/2}$ anticrossings. Derivative of the left QPC conductance is plotted vs magnetic field and initial detuning for a pulse of 50 ns duration Gaussian filtered with a 12 ns rise time and amplitude $(\delta V_1, \delta V_2) = (-8.5, 10)$ mV.

four differential equations are solved using the Runge-Kutta method.

We calibrated the exchange energies J_{LC} (J_{RC}) and interdot couplings to be used in the model using a standard technique [10]. We mapped out the magnetic field position at which the doublet $\Delta'_{1/2}$ state crossed the dispersionless

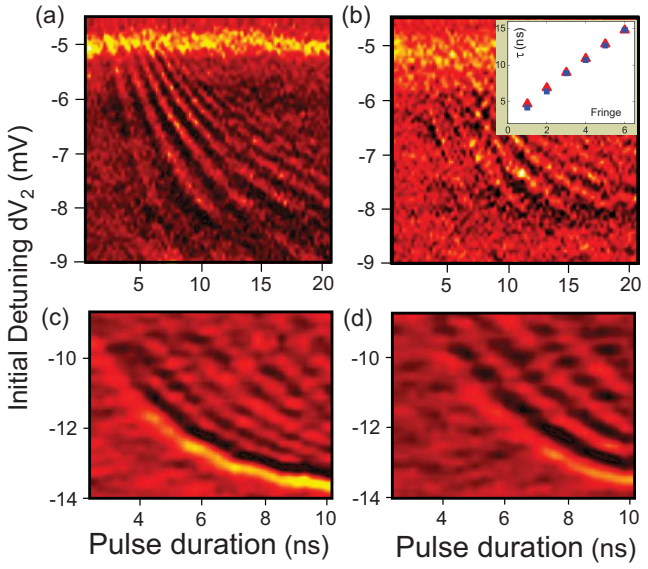

FIG. 3. (Color online) Contrasting magnetic field dependencies of exchange (a), (b) and LZS (c), (d) fringes. The experimental derivative of the left QPC conductance is plotted vs pulse duration and detuning at (a) 100 mT, (b) 20 mT, (c) 40 mT, (d) 25 mT. For (a), (b) [(c), (d)] a rectangular pulse of duration τ Gaussian filtered with a 1.0 [4.0] ns rise time and amplitude $(\delta V_1, \delta V_2) = (-8, 10)$ [$(-8.5, 10)$] mV traverses the charge transfer line between (2,0,1) and (1,1,1). Black is low, orange is medium, and yellow is high transconductance. Inset to (b) compares extracted dark fringe positions from (a), (b) at -7 mV detuning; a: triangle, b: square.

quadruplet $Q_{3/2}$ state (the $Q_{3/2}$-$Q_{1/2}$ spacing is the Zeeman energy). In this measurement a 50 ns pulse duration was used, long relative to typical dephasing times (10–20 ns) to suppress coherent oscillations. A typical map is shown in Fig. 2. The labels L, D, and e-L indicate typical locations for observing, respectively, LZS, double beam splitter, and exchange-enabled LZS oscillations for shorter pulse durations. This curve is fitted with a function containing the interdot couplings to provide the parameters for the energy diagram used in the calculations [10].

Typical interdot couplings for this work were around 10–20 μeV. Hyperfine couplings were estimated around 0.1–0.2 μeV. The minimum exchange splitting $J_{\min} = (\Delta_{1/2} - \Delta'_{1/2})_{\min}$ in these experiments occurs near zero detuning with values in the range 0.28–0.52 μeV.

III. EXCHANGE AND LZS OSCILLATIONS

Here we review how we distinguish between the two most commonly observed coherent phenomena in the triple quantum dot, the all-exchange and Landau-Zener-Stückelberg oscillations. In a recent paper [11] we established that coherent oscillations related to either AE or LZS [13] processes could be activated in our device by suitable pulses. These are indicated by circulation symbols in Fig. 1(c). The LZS beam splitting (by analogy to optics) occurred on passage through hyperfine split doublet/quadruplet anticrossings marked with blue circles in the (1,1,1) region. The phase accumulation after the beam splitting between the quantum state components is a function of the evolution time and the magnitude of the level separation [10,13,18–21]. This separation depends both on the detuning and the magnetic field (via Zeeman shifts to the $Q_{3/2}$ state). On the other hand, the magnitude of the AE qubit level splitting, $\Delta_{1/2}$-$\Delta'_{1/2}$, is independent of the external magnetic field. Therefore, one can use the LZS and AE respective magnetic field dependencies to qualitatively assess the consequence of the applied pulses [11,12].

To selectively activate the AE qubit oscillations one should apply a pulse with a very short rise time (1 ns). In this case, as the pulse crosses the hyperfine split anticrossings the population of the initial state remains close to unity and only the exchange interaction leads to spin rotation. An additional z-hyperfine coupling between the $\Delta_{1/2}/Q_{1/2}$ states can be made irrelevant either through the use of very short pulse durations or by using devices defined in isotopically pure Si^{28} where hyperfine effects are absent. This subtlety has been examined elsewhere [12]. To illustrate the magnetic field signature for this AE qubit in Figs. 3(a), 3(b) we compare experimental exchange fringes for two values of magnetic field for a short pulse rise time of 1.0 ns. The positions of the fringes are independent of a fivefold increase in magnetic field (see inset), confirming them to be due to exchange rotation (the AE qubit). By comparison, at larger (4 ns) pulse rise times the hyperfine driven LZS fringes associated with the $Q_{3/2}/\Delta'_{1/2}$ anticrossings are strongly magnetic field dependent as shown in Figs. 3(c), 3(d) where the fringe period almost halves between fields of 25 and 40 mT. In all panels of Fig. 3 the pulse peak reaches the center of the (1,1,1) region for an initial detuning of about -10 mV. The AE (LZS) fringes are observed beyond (before) this point.

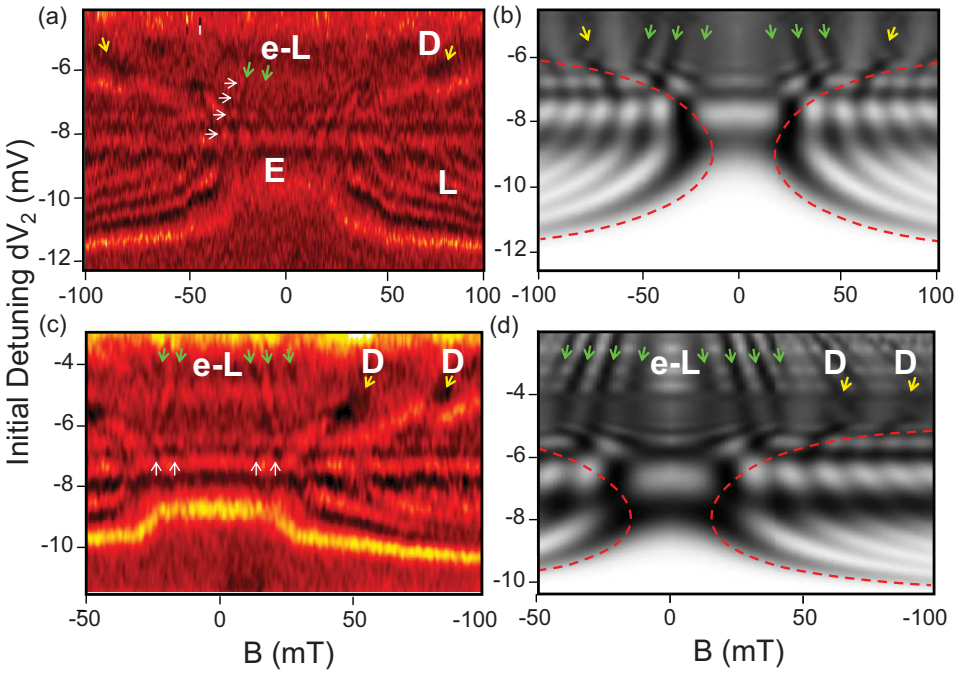

FIG. 4. (Color online) (a) Experimental derivative of the left QPC conductance as a function of dV_2 and magnetic field B for a 13 ns rectangular pulse Gaussian filtered with an 8 ns rise time and amplitude $(\delta V_1, \delta V_2) = (-8.5, 10.0)$ mV, the (1,1,1) region was 8 mV wide. $J_{\min} = 0.36\,\mu$eV. L: LZS fringes, e-L: exchange-enabled LZS, D: double beam splitter, E: exchange. (b) Calculated probability $P_{\bar{D}'_{1/2}}$. Black is low, white is high. Dashed line is the experimental locus of anticrossings that underpins the calculations. (c) Same as (a) but with 6 mV (1,1,1) region width, $J_{\min} = 0.28\,\mu$eV, pulse amplitude $(\delta V_1, \delta V_2) = (-6.8, 8.0)$ mV. (d) Calculated probability $P_{\bar{D}'_{1/2}}$. Black is low, white is high. Dashed line as in (b). White, green, and yellow arrows are explained in the text.

Such a description of the qubit evolution is, however, incomplete. This can be clearly seen by utilizing the different magnetic field dependences of the interactions as in Figs. 4(a)–4(d) where we show the experimental magnetic field dependence for a fixed 13 ns rectangular pulse duration (convoluted with a 8 ns rise time) together with results from modeling for two different (1,1,1) region widths (to illustrate the universal nature of these effects). Graphs plotted this way reveal a remarkably rich collection of interference signatures, which are qualitatively reproduced in the modeling. As a reference point the dotted line in the model data indicates the loci of the two anticrossings between $Q_{3/2}$ and $\Delta'_{1/2}$ states. The modulation relating to the LZS and AE qubits are clearly visible in both cases. The LZS oscillations originating from the left-center anticrossing are marked with an L. The field-independent horizontal stripes passing through zero magnetic field, marked E, are the all-exchange (AE) qubit oscillations. Only a few AE stripes are visible in these experimental plots. This is to be expected as the level spacing between $\Delta_{1/2}$ and $\Delta'_{1/2}$ grows rapidly away from the point of closest approach [middle of Fig. 1(c)] resulting in faster oscillations vs detuning, prone to experimental quenching by charge noise effects (included in the modeling as detuning averaging). We note that the lowest (dark) exchange fringe near -8 mV detuning occurs where the axis of rotation has not completed its shift with peak detuning by 120° on the $\bar{D}'_{1/2}/\bar{D}_{1/2}$ Bloch sphere of Fig. 1(b) (as right-center exchange dominates over left-center exchange) and involves a π rotation approximately around the x axis (the eigenstates of this Bloch sphere correspond to the region where the pulse starts and where the readout is performed). The remaining exchange fringes relate to state vector rotations on the Bloch sphere around the axis corresponding to the $D'_{1/2}/D_{1/2}$ states [the right side of Fig. 1(c)] at 120° to the $\bar{D}'_{1/2}/\bar{D}_{1/2}$ axis [see Fig. 1(b)] [9,11].

Two additional types of interference in the data have not previously been observed in experiment and are the main subject of this paper. These are the double beam splitter (DBS) and the exchange-enabled LZS (e-LZS) interferences. Although these objects are hard to observe (see discussion below) it is important to understand them because they represent potential leakage pathways from the all-exchange qubit [11,12].

IV. DOUBLE BEAM SPLITTER AND EXCHANGE-ENABLED LZS

Just beyond the right-side anticrossing, broad (in magnetic field) dark fringes are marked with a D and yellow arrows in Figs. 4(a), 4(c). Their origin (obtained from an analysis of the model) is an interplay between two coupled spin interferometers, one initiated after the left anticrossing and the other after the right anticrossing [see Figs. 5(a), 5(b)] for pulses that pass through both. We refer to this as a double beam splitter, DBS [11,13]. It should be stressed that both interferometers involve the same constituent quantum states, $Q_{3/2}$ and $\Delta'_{1/2}$, which are brought to anticross twice as a function of detuning by the opposite detuning variation of the two exchange parameters (i.e.,J_{RC} increases as J_{LC} decreases and vice versa). The resultant phase behavior is based on a complex interference between these two interrelated evolutions. Interestingly these two behaviors involve rotations on the Bloch sphere in contrary directions and possess opposite dependencies on magnetic field (a trivial consequence of the energy level diagram). A related quantum interference effect has also recently been encountered in the superconducting qubit platform [22]. In Figs. 5(a), 5(b) schematics are drawn for two different magnetic fields where the origin of the field dependence is the Zeeman shift of the $Q_{3/2}$ state relative to the $\Delta'_{1/2}$ state. At larger magnetic field [Fig. 5(b)] the $Q_{3/2}$ state

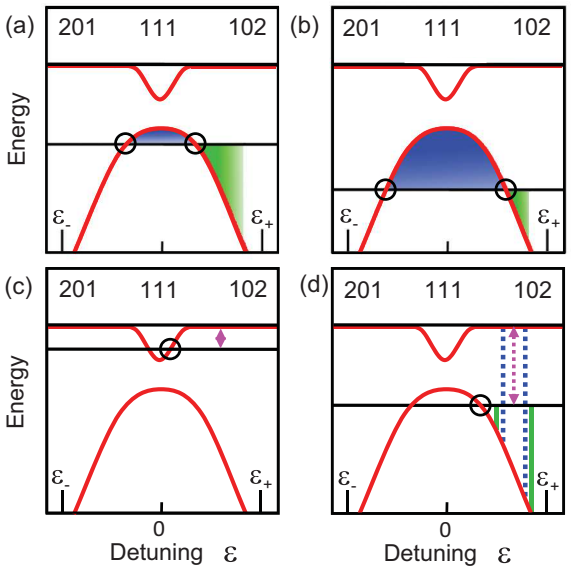

FIG. 5. (Color online) (a), (b) Schematic illustration of double beam splitter interference due to different magnetic field dependencies of left- and right-side oscillations; (a) lower, (b) higher magnetic field. (c), (d) Schematic illustration of exchange enabled LZS where $Q_{3/2}$ cuts (c) $\Delta_{1/2}$ and (d) $\Delta'_{1/2}$.

anticrosses with the $\Delta'_{1/2}$ state at points separated by a larger detuning range. For a pulse of fixed shape to the same detuning point beyond the right-side anticrossing, the accumulated phase acquired during passage of the pulse between the anticrossings [blue area in Figs. 5(a), 5(b)] increases with magnetic field as it takes the form $\phi = \frac{1}{\hbar}\int\{E_{\Delta'}[\epsilon(t)] - E_{Q_{3/2}}\}dt$. Likewise, a similar phase term (but with opposite sign) applies to the time spent by the pulse beyond the right anticrossing [green area in Figs. 5(a), 5(b)] and the combination of these terms leads to the rather broad and indistinct fringes marked with D and yellow arrows in Figs. 4(a), 4(c). Similar fringes are observed in the calculations, Figs. 4(b), 4(d). A rough estimate of the spacing of the fringes (in magnetic field) can be made from the total phase accumulation between the anticrossings using the above expression for ϕ. For the pulse conditions used here this yields a magnetic field spacing of between 20–30 mT, which is in reasonable agreement with the spacing between the D symbols in Figs. 4(c), 4(d). To illustrate the interactions involved we plot in Fig. 6(c) the evolution of the diagonals of the density matrix during the pulse at a point near the left D marker in Fig. 4(d) (56 mT, −3 mV) corresponding to a double beam splitter fringe. To clarify this we switch off the exchange interaction by showing the result calculated in the $\Delta'_{1/2}$ rather than the $\bar{D}'_{1/2}$ basis. This eliminates the rapid exchange oscillations. If we do not do this the action during the pulse is obscured by the exchange oscillations (see discussion below). On each side of the pulse peak we see the $\Delta'_{1/2}/Q_{3/2}$ fractions oscillate as the pulse passes between the hyperfine anticrossings. Since both anticrossings in this interference effect involve the same constituent $Q_{3/2}$ and $\Delta'_{1/2}$ states this can be considered as a rather unusual qubit with quite complicated properties.

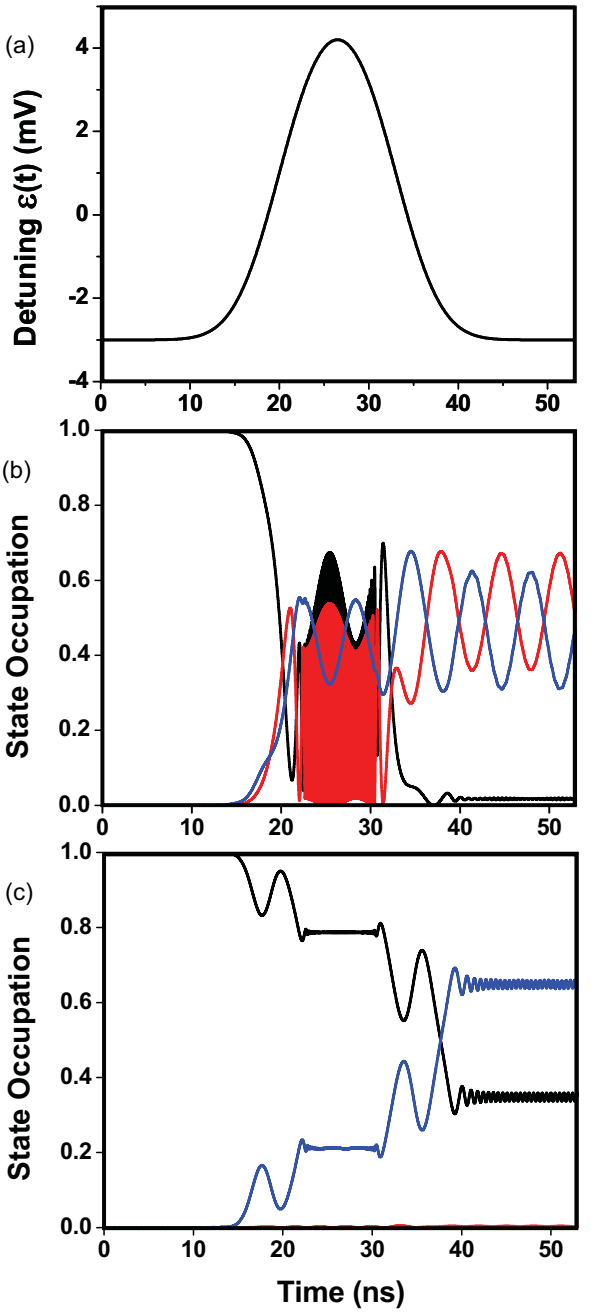

FIG. 6. (Color online) (a) Detuning pulse as a function of time corresponding to the calculation of Fig. 4(d). (b) Calculated state occupation probabilities as a function of time for pulse shown in (a) for a pulse starting at gate detuning −3 mV with $B = 27$ mT, corresponding to a $\Delta_{1/2}/Q_{3/2}$ fringe. Black: $\bar{D}'_{1/2}$; red: $\bar{D}_{1/2}$; blue: $Q_{3/2}$. (c) Calculated state occupation probabilities as a function of time for a pulse starting at gate detuning −3 mV with $B = 56$ mT, corresponding to a double beam splitter fringe. Black: $\Delta'_{1/2}$; blue: $Q_{3/2}$. This plot is calculated with the exchange interaction switched off (working in the $\Delta'_{1/2}$ basis) to clarify the double beam splitter effect during the pulse sequence. Both figures are calculated without (z)-hyperfine interactions for clarity. Phase accumulation in (c) occurs primarily near the $\Delta'_{1/2}/Q_{3/2}$ anticrossings around the 20 ns (outgoing) and 35 ns (returning) parts of the pulse.

A second evolution is observed experimentally, marked with e-L and green arrows in Fig. 4(c) and also visible in Fig. 4(a), and reproduced in the theory. These fringes move to lower magnetic field as the detuning is increased and this indicates that they involve the energy spacing between (and thus a qubit of) the $\Delta_{1/2}$ and $Q_{3/2}$ states. A comparison with the model reveals the origin of these fringes as a direct interplay and quantum interference between the AE and LZS modulations. We refer to these as exchange-enabled LZS or e-LZS. A close examination of the data in Figs. 4(a), 4(c) reveals that around zero magnetic field the AE horizontal lines are modulated [white arrows in Fig. 4(c)]. The modulations at various AE lines combine to form the fringes [white/green arrows in Fig. 4(a)]. However, the fringes are also observed at less negative detunings where the AE are erased by charge noise (see below). Most of the e-LZS fringes are observed for smaller magnetic fields, as in Fig. 5(c). In this situation the AE qubit coherently populates the $\Delta_{1/2}$ state at positive detuning in a time dependent manner related to AE evolution. This leads to beam splitting with resultant LZS behavior at the right-side anticrossing with the $Q_{3/2}$ state. As a result the evolution involves an interference effect between the two qubits, AE and LZS. It is important to note that the LZS level spacing $E_{\Delta_{1/2}}$-$E_{Q_{3/2}}$ becomes rapidly independent of detuning away from zero detuning giving rise to almost vertical resonances in Figs. 4(a), 4(c). At higher magnetic fields where the $Q_{3/2}$ intersects $\Delta'_{1/2}$ an equivalent interference mechanism exists [see Fig. 5(d)], which leads to coherent behavior with the same $\Delta_{1/2}$-$Q_{3/2}$ level spacing. These fringes are observed in the model over a wider field range than in the experiment. In Fig. 6(b) we show the state evolution at a point near the e-L marker in Fig. 4(d) (27 mT, −3 mV) corresponding to a e-LZS ($\Delta_{1/2}/Q_{3/2}$) fringe. The rapid oscillation near the pulse peak is the exchange oscillation due to the large $\Delta'_{1/2}$-$\Delta_{1/2}$ energy spacing at this position. Following this almost all the weight is fed into the hyperfine $\Delta_{1/2}/Q_{3/2}$ interaction and remains after the pulse is completed in the absence of (z)-hyperfine coupling. In the presence of such coupling there is leakage into $Q_{1/2}$.

The observation of hyperfine-induced oscillations by pulsing to the far side of a triple quantum dot stability diagram presents difficulties that complicate comparisons with theoretical calculations. The e-LZS ($\Delta_{1/2}/Q_{3/2}$) fringes and the double beam splitter interference fringes [11] are observed on a background of dense exchange fringes, washed out by charge noise, and heavy hyperfine leakage to the $Q_{1/2}$ state. One particular issue is the display of fringes using the derivative with respect to detuning as is done for all of the experimental data in this work. This removes large background variations in the raw signal but suppresses fringes that are asymptotically independent of detuning as is the case for the fringes of particular interest here. In principle, a derivative with respect to magnetic field would solve this (while making exchange fringes essentially invisible) but, due to drift between successive detuning scans at different fields, is not practical with our current system.

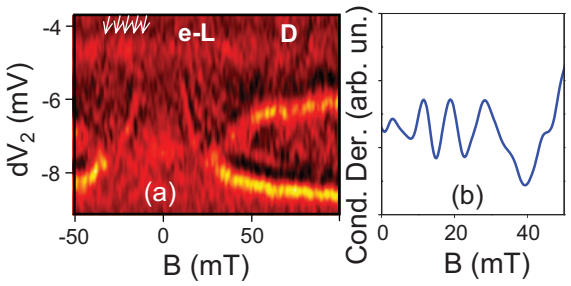

FIG. 7. (Color online) (a) Experimental derivative of the left QPC conductance as a function of dV_2 and magnetic field B for a 13 ns rectangular pulse Gaussian filtered with 8 ns rise time and amplitude (−6.8,8.0) mV. (1,1,1) region width was 4.4 mV. $J_{\min} = 0.52\,\mu$eV. (b) B dependence from (a) detuning average around $dV_2 = -5.6$ mV to show e-LZS fringes.

Empirically we find that e-LZS are more visible under conditions where the (1,1,1) region is small (with a large minimum exchange splitting but where AE and LZS fringes are especially subject to charge noise). Figure 7(a) shows data for the highest $J_{\min}$ for which we were able to observe coherent modulations, 0.52 μeV. We also show a detuning-averaged line plot in Fig. 7(b) to make the e-LZS fringes clearer. For the 8 ns rise time we observe only weak signatures of the AE and LZS qubits. Despite this, a number of e-LZS are visible (arrows for negative B are shown to guide the eye). We speculate that this surprising behavior is related to the fact that the e-LZS modulations exist in a decoherence-free subspace for charge noise since the level spacing between $Q_{3/2}$ and $\Delta_{1/2}$ becomes detuning independent in this range, even though the individual AE and LZS qubits are very sensitive to detuning. This is illustrated in schematic Fig. 5(d) where charge noise (represented by two different detunings) results in different splittings for the component qubits but the resultant interference involves a constant splitting. Analogous behavior occurs for the interference in Fig. 5(c).

V. CONCLUSION

In conclusion we have observed and explained two novel quantum interference phenomena that occur between three-spin states in a TQD. This augments the catalogue of coherent hyperfine-coupled three-spin oscillations that represent potential leakage paths for the exchange-only qubit in this system.

ACKNOWLEDGMENTS

We acknowledge discussions with W. A. Coish, L. Gaudreau, M. Pioro-Ladrière, A. Clerk, and D. G. Austing. A.S.S. acknowledges funding from NSERC and CIFAR.

Authors G.P.-L. and J.T. contributed equally to this work.

[1] D. P. DiVincenzo, D. Bacon, J. Kempe, G. Burkard, and K. B. Whaley, Nature (London) **408**, 339 (2000).

[2] A. D. Greentree, J. H. Cole, A. R. Hamilton, and L. C. L. Hollenberg, Phys. Rev. B **70**, 235317 (2004).

[3] B. Michaelis, C. Emary, and C. W. J. Beenakker, Europhys. Lett. **73**, 677 (2006).

[4] M. Busl, R. Sanchez, and G. Platero, Phys. Rev. B **81**, 121306(R) (2010).

[5] P. Hawrylak and M. Korkusinski, Solid State Commun. **136**, 508 (2005).
[6] L. Gaudreau, A. Kam, G. Granger, S. A. Studenikin, P. Zawadzki, and A. S. Sachrajda, Appl. Phys. Lett. **95**, 193101 (2009).
[7] G. Granger, L. Gaudreau, A. Kam, M. Pioro-Ladrière, S. A. Studenikin, Z. R. Wasilewski, P. Zawadzki, and A. S. Sachrajda, Phys. Rev. B **82**, 075304 (2010).
[8] D. Schroer, A. D. Greentree, L. Gaudreau, K. Eberl, L. C. L. Hollenberg, J. P. Kotthaus, and S. Ludwig, Phys. Rev. B **76**, 075306 (2007).
[9] E. A. Laird, J. M. Taylor, D. P. DiVincenzo, C. M. Marcus, M. P. Hanson, and A. C. Gossard, Phys. Rev. B **82**, 075403 (2010).
[10] L. Gaudreau, G. Granger, A. Kam, G. C. Aers, S. A. Studenikin, P. Zawadzki, M. Pioro-Ladrière, Z. R. Wasilewski, and A. S. Sachrajda, Nat. Phys. **8**, 54 (2011).
[11] G. C. Aers, S. A. Studenikin, G. Granger, A. Kam, P. Zawadzki, Z. R. Wasilewski, and A. S. Sachrajda, Phys. Rev. B **86**, 045316 (2012).
[12] J. Medford, J. Beil, J. M. Taylor, S. D. Bartlett, A. C. Doherty, E. I. Rashba, D. P. DiVincenzo, H. Lu, A. C. Gossard, and C. M. Marcus, Nat. Nanotech. **8**, 654 (2013).
[13] J. R. Petta, H. Lu, and A. C. Gossard, Science **327**, 669 (2010).
[14] M. Field, C. G. Smith, M. Pepper, D. A. Ritchie, J. E. F. Frost, G. A. C. Jones, and D. G. Hasko, Phys. Rev. Lett. **70**, 1311 (1993).
[15] J. R. Petta, A. C. Johnson, J. M. Taylor, E. A. Laird, A. Yacoby, M. D. Lukin, C. M. Marcus, M. P. Hanson, and A. C. Gossard, Science **309**, 2180 (2005).
[16] J. M. Taylor, J. R. Petta, A. C. Johnson, A. Yacoby, C. M. Marcus, and M. D. Lukin, Phys. Rev. B **76**, 035315 (2007).
[17] K. Ono, D. G. Austing, Y. Tokura, and S. Tarucha, Science **297**, 1313 (2002).
[18] H. Ribeiro and G. Burkard, Phys. Rev. Lett. **102**, 216802 (2009).
[19] H. Ribeiro, J. R. Petta, and G. Burkard, Phys. Rev. B **82**, 115445 (2010).
[20] J. Särkkä and A. Harju, New J. Phys. **13**, 043010 (2011).
[21] S. Shevchenko, S. Ashhab, and F. Nori, Phys. Rep. **492**, 1 (2010).
[22] G. Sun, X. Wen, B. Mao, J. Chen, Y. Yu, P. Wu, and S. Han, Nat. Commun. **1**, 51 (2010).